Measurement of the $^2P_{1/2}$-$^2P_{3/2}$ fine-structure splitting in fluorinelike Kr, W, Re, Os, and Ir

Galen O'Neil,[1,*] Samuel Sanders,[2,3] Paul Szypryt,[1,4] Dipti,[2] Amy Gall,[5] Yang Yang,[2,3] Samuel M. Brewer,[6] Randy Doriese,[1] Joe Fowler,[1,4] Aung Naing,[7,2] Daniel Swetz,[1] Joseph Tan,[2] Joel Ullom,[1] Andrey V. Volotka,[8] Endre Takacs,[2,3] and Yuri Ralchenko[2,†]

[1]*National Institute of Standards and Technology, Boulder, Colorado 80303, USA*
[2]*National Institute of Standards and Technology, Gaithersburg, Maryland 20899, USA*
[3]*Clemson University, Department of Physics and Astronomy, Clemson, South Carolina 29634, USA*
[4]*University of Colorado, Department of Physics, Boulder, Colorado 80309, USA*
[5]*Harvard Smithsonian Astrophysical Observatory, Cambridge, Massachusetts 02138, USA*
[6]*Department of Physics, Colorado State University, Fort Collins, Colorado 80523, USA*
[7]*University of Delaware, Department of Physics and Astronomy, Newark, Delaware 19716, USA*
[8]*Helmholtz Institute Jena, Jena 07743, Germany*

(Received 16 June 2020; accepted 11 August 2020; published 2 September 2020)

Quantum electrodynamics (QED) is currently considered to be one of the most accurate theories of fundamental interactions. As its extraordinary precision offers unique scientific opportunities, e.g., search for new physics, stringent experimental tests of QED continue to be of high importance. To this end, highly charged ions represent an exceptional test-bed due to enhanced QED effects. Recently, forbidden transitions in F-like ions have been analyzed to few ppm precision, resolving previous discrepancies between theory and experiment. Here we further test the accuracy of QED calculations with three new (Re, Os, Ir), and two improved (Kr, W) measurements of the $^2P_{1/2}$-$^2P_{3/2}$ transition energy in F-like ions using the NIST electron-beam ion trap and extreme-ultraviolet and x-ray spectrometers. Good agreement between theoretical and experimental energies is found for all considered elements.

DOI: 10.1103/PhysRevA.102.032803

I. INTRODUCTION

In comparison with neutral atoms or low-charged ions, many physical phenomena are greatly enhanced in highly charged ions (HCIs) [1]. Relativistic and Breit effects, quantum-electrodynamic (QED) corrections, and violations of various selection rules are all known to become more significant and influential in the structure and radiative properties of HCIs. Notwithstanding the general enhancements, some atomic systems offer easier avenues for exploration of those effects. For instance, Na- and Li-like ions with one electron outside closed shells proved to be very beneficial for testing QED predictions for high-Z elements [2–4]. While electron correlations can be substantial even in multi-electron HCIs, the quasi-one-electron systems exhibit suppressed correlations and thus better applicability for identification of relativistic and QED effects.

Another group of ions with reduced correlation effects belong to the F-like isoelectronic sequence. The Layzer complex of the negative-parity $n = 2$ configurations contains only the ground-state (g.s.) configuration $1s^22s^22p^5$ and thus electron correlations are significantly suppressed for the corresponding atomic states. This effect was referred to as the "Layzer quenching" in Ref. [5] where it was proposed to explore the magnetic-dipole ($M1$) transition $^2P_{1/2}$-$^2P_{3/2}$ within the g.s. configurations of F-like ions to benchmark different approaches for calculation of Breit and QED effects. Although the theoretical results in Ref. [5] were not fully successful in explaining the observed wavelengths of the $M1$ lines along the sequence, the recent work [6] implementing *ab initio* calculations of QED radiative corrections was able to resolve the discrepancies between theory and experiment. Recently, in Ref. [7], it has been further confirmed with the QED corrections evaluated with the model potential approximation.

Here we present extreme-ultraviolet (EUV) and x-ray spectroscopic measurements of the $^2P_{1/2}$-$^2P_{3/2}$ transition in five elements in the F-like isoelectronic sequence, and interpret these measurements as tests of QED calculations of the transition energy. We used the electron-beam ion trap (EBIT) operating at the National Institute of Standards and Technology (NIST) to produce F-like ions of Kr, W, Re, Os, and Ir. We studied the $^2P_{1/2}$-$^2P_{3/2}$ fine-structure radiation with two different spectrometers, namely, a wavelength dispersive EUV spectrometer for the F-like Kr line at 55 eV, and the energy-dispersive NIST EBIT transition-edge sensor spectrometer (NETS [8]) for the W, Re, Os, and Ir lines from 1390 to 1670 eV. The spectra are analyzed to find the energy of the $^2P_{1/2}$-$^2P_{3/2}$ magnetic-dipole ($M1$) line with a careful evaluation of multiple sources of systematic uncertainty. The results are summarized in Table I, details of the data acquisition and analysis are described in Sec. II, and theoretical

*galen.oneil@nist.gov
†yuri.ralchenko@nist.gov

TABLE I. The energies of the F-like $^2P_{1/2}$-$^2P_{3/2}$ lines measured for various elements in this work and previous work and as calculated by QED theory. For Kr and W, previous experimental energy values are from Refs. [9,10] and theory energy values are from Ref. [6]. Theory energy values for Re, Os, and Ir are discussed in Sec. III [6]. For energy values from this work, the statistical uncertainty is followed by the systematic uncertainty.

		Energy (eV)		
Element	Z	This work	Prev. expt.	Theory
Kr	36	55.3523(9)(11)	55.352(7)	55.356(3)
W	74	1389.51(21)(9)	1388.87(60)	1389.38(8)
Re	75	1478.37(11)(9)		1478.31(9)
Os	76	1572.12(26)(21)		1571.91(9)
Ir	77	1670.29(22)(18)		1670.40(10)

calculations and comparisons between theory and experiment are presented in Sec. III.

II. METHODS

A. Acquisition of spectra

1. Electron-beam ion trap

The NIST EBIT is a laboratory instrument for producing and studying highly charged ions [11,12]. An electron beam with a maximum current of 150 mA is compressed to a narrow cylinder with radius of ≈35 μm. Atoms that interact with the beam become ionized, radial confinement results from attraction to the electron beam, and electric fields from nearby electrodes provide axial confinement. The population of ions and excited states generated in the EBIT is primarily determined by the current density of the electron beam, the kinetic energy of the electrons, and the atoms injected to interact with the electron beam. Photons emitted from these ions were detected with the EUV spectrometer and the NETS x-ray spectrometer.

2. Extreme-ultraviolet spectrometer

The EUV spectrometer collects photons with a grazing-incidence gold-coated spherical mirror 48 cm from the electron beam. Photons are focused onto a narrow slit and subsequently dispersed by a gold-coated flat-field reflection grating with 1200 grooves/mm. A liquid-nitrogen-cooled (LN_2-cooled) CCD detector records two-dimensional (2D) spectra in 60 s increments. Spectra were hardware binned before readout to produce one-dimensional (1D) spectra in the energy-dispersive direction. Further processing of the data includes a routine to remove the influence of cosmic rays. The slit opening was set to 2 cm, which results in a full width at half maximum (FWHM) resolving power of 580, limited by the size of the overlap between the electron beam and the ion cloud in the EBIT. Reference [13] provides significantly more detail on the EUV spectrometer. Additional details can also be found in previous studies that used this instrument (e.g., Refs. [2,14,15] and references therein).

3. X-ray spectrometer

NETS consists of 192 pixels, each of which is a transition-edge sensor (TES) spectrometer. A brief description of NETS follows and significantly more information is available in Ref. [8]. Each pixel consists of a superconducting element with a transition temperature of 110 mK, and a 1-μm-thick Au x-ray absorber. When an x-ray is absorbed by a pixel, the resulting temperature rise causes the resistance of the TES to increase, and due to the applied voltage bias, there is a transient current reduction referred to as a *pulse*. In the 1000 to 2000 eV range of interest in this work, the height of the pulse is proportional to the energy of the incident x-ray to within a few percent, and the energy of each incident x-ray can be measured with a full-width-at-half-maximum (FWHM) energy resolution of 3.8 eV.

4. Experimental protocol

In the present experiments, a metal vapor vacuum arc (MeVVA [16]) external ion source was used to inject singly charged Fe, W, Re, Os, and Ir into the EBIT, and a gas injection system provided CO_2, Ne, and Kr neutral gases for calibration and measurement purposes. Spectra were acquired on three separate days. One day, x-ray spectra of W and Re were acquired with a beam energy of 20 kV, interspersed with Ne spectra for calibration purposes. Another day, x-ray spectra of Os and Ir were acquired with a beam energy of 21 kV. On a final day EUV spectra of Kr were acquired at five beam energies from 2.5 to 5.5 kV. EUV spectra of Ne, CO_2, and Fe were acquired the same day. X-ray and EUV photons generated by the interaction of the electron beam with injected atoms were detected by the NETS and the EUV spectrometer, respectively. A LN_2 tank near the EBIT, used to cool the electron-beam collector, must be filled from a larger remote tank every ≈90 minutes. The EBIT electron beam was turned off during the fills, which take ≈15 minutes. During the LN_2 fills, NETS observed secondary x-rays from a *calibration target* illuminated by a commercial x-ray source. At the start of each LN_2 fill, the calibration target was moved in front of the NETS input window with a manually operated linear-motion vacuum-feedthrough, and the commercial x-ray source was energized. This process was reversed at the end of each LN_2 fill.

B. Extreme ultraviolet spectrometer data analysis

The relationship between bin position and incident photon wavelength in the EUV spectrometer is modeled as a third-order polynomial. Many strong and well-known spectral lines from Ar, Ba, C, Fe, Kr, Ne, O, and Xe [17] are used to determine the coefficients of this polynomial. The centroid

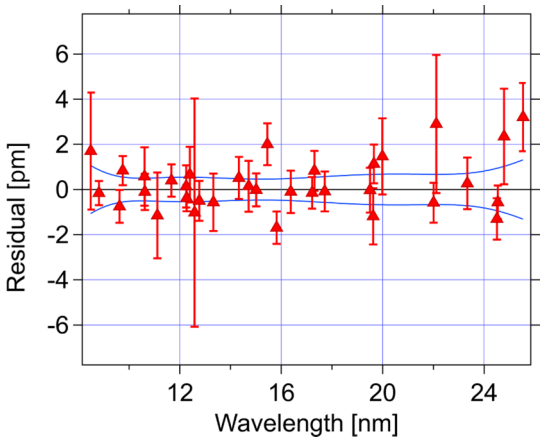

FIG. 1. Residuals (triangles) between the fitted wavelengths and published wavelengths of the calibration lines as a function of the wavelength as determined by the calibration procedure. The error bars are the quadrature sum of the statistical uncertainty, the published centroid position uncertainty, and σ_{EUVsys} explained in the text. The 95% confidence intervals are shown as the blue traces. These residuals are for calibration sources taken before the shift of the spectrometer.

energies of these lines are determined by fitting Gaussian lineshapes to the data. When fitting for the coefficients of the calibration polynomial, each centroid energy is weighted by the quadrature sum of the statistical uncertainty from the centroid fit, the published line wavelength uncertainty, and a single shared systematic uncertainty value, σ_{EUVsys}. The value of σ_{EUVsys} is determined such that the reduced chi-squared value of the calibration polynomial fit is 1. Some elements are incidentally present in the EBIT at high enough concentrations to use for calibration lines. These elements are residual Xe from past injection, Ba from the electron-gun surface, and Ar from the ion pump of the EUV spectrometer. The difference between the literature values of the calibration line centroids and the value assigned by our calibration procedure is shown in Fig. 1. During the experiment, the EUV spectrometer was accidentally bumped, resulting in a slight shift of the spectral centroids by approximately a quarter of a channel unit. Therefore, two separate spectral calibrations were performed, one before and one after the shift. We compared about 40 centroid positions before and after the shift and found the shift size was consistent across all lines, to our ability to measure it. The value of σ_{EUVsys} was found to be 0.0003 nm before and after the shift.

The Kr spectra were recorded at five electron-beam energies straddling the ionization potential of the F-like Kr charge state. Two of these spectra are shown in Fig. 2. Total collection times were 5, 10, 40, 100, and 30 minutes for the electron-beam energies 2.5, 3.0, 3.5, 4.0, and 5.5 keV, respectively. Given that the ionization potential of Ne-like Kr charge state is 2.9289 ± 0.0017 keV [17], the spectral lines observed with electron-beam energies of 2.5 and 3.0 keV are not attributed to F-like Kr: 2.5 kV is not sufficient to ionize the Ne-like Kr while 3.0 kV, on account of the space-charge effect, should result in a negligible number of F-like ions in the trap. For the higher beam energies, the F-like Kr $^2P_{1/2}$-$^2P_{3/2}$ $M1$ line was indeed observed. The spectrum recorded at 5.5 keV

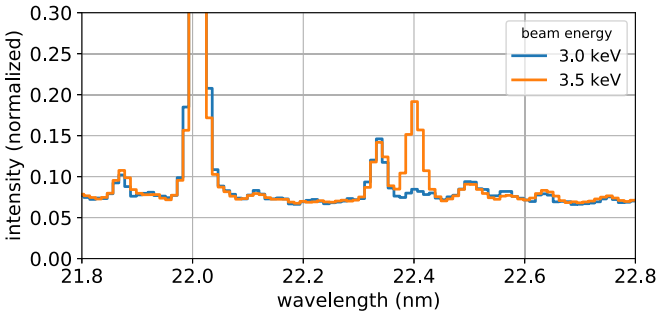

FIG. 2. Spectra observed with the EUV spectrometer with Kr injected into the EBIT at 3.0 and 3.5 keV electron-beam energies, shown for wavelengths near the transition of interest. The line near 22.4 nm in that appears at beam energy 3.5 keV is assigned to the F-like Kr $^2P_{1/2}$-$^2P_{3/2}$ transition. This line is present with slightly reduced intensity in the 4.0 and 5.5 keV spectra, and is not present in the 2.0 keV spectrum. The collected spectra span 7.6 to 26.3 nm, and the shown spectra are normalized by the sum of all counts in that range with an additional shared scaling factor to make the numbers of order one. The bin sizes are ≈0.011 nm for the range shown in this figure.

was measured before the spectrometer shift, where all other beam energies were recorded after the shift. We fit the line wavelength separately for each of the beam energies in which it appears, then take a weighted average of those wavelengths including only the statistical uncertainty determined by the fitting procedure, giving the result 22.3991 ± 0.0004 nm. We estimate the systematic uncertainty as the quadrature sum of σ_{EUVsys}, and the one sigma confidence interval (0.0003 nm) calculated from the calibration curve at the measured wavelength. The transition energy and uncertainties in eV are shown in Table I.

C. NIST EBIT transition-edge sensor spectrometer data analysis

Here we describe in detail the analysis of the Re x-ray spectra from the NETS. The W data were taken on the same day and analyzed in the same way as the Re data. Section II C describes how the analyses of the Ir and Os spectra differ from the Re case. We recorded a 1000 sample (4.8 μs/sample) pulse record for each x-ray event. The following steps were performed independently for each pixel to calculate a *corrected pulse height* from each of these pulse records. (1) We generated low-noise pulse-height estimates by using a filter which is designed to be insensitive to the pulse-shape variation that results from differences in x-ray arrival-time relative to the most recent sampling time. (2) We performed a series of corrections attempting to remove the correlations between time and pulse height, quiescent current and pulse height, and subsample arrival time and pulse height. The parameters required for these corrections are determined with an optimization algorithm which uses decreased spectral entropy as an indicator of improved energy resolution. (3) Fit for the Al $K\alpha$ pulse height each time the x-ray tube source was operated. A quadratic fit to Al $K\alpha$ pulse height vs time is used to perform an additional correction to further reduce correlations between time and pulse height. The first two steps are described in more detail in Ref. [18].

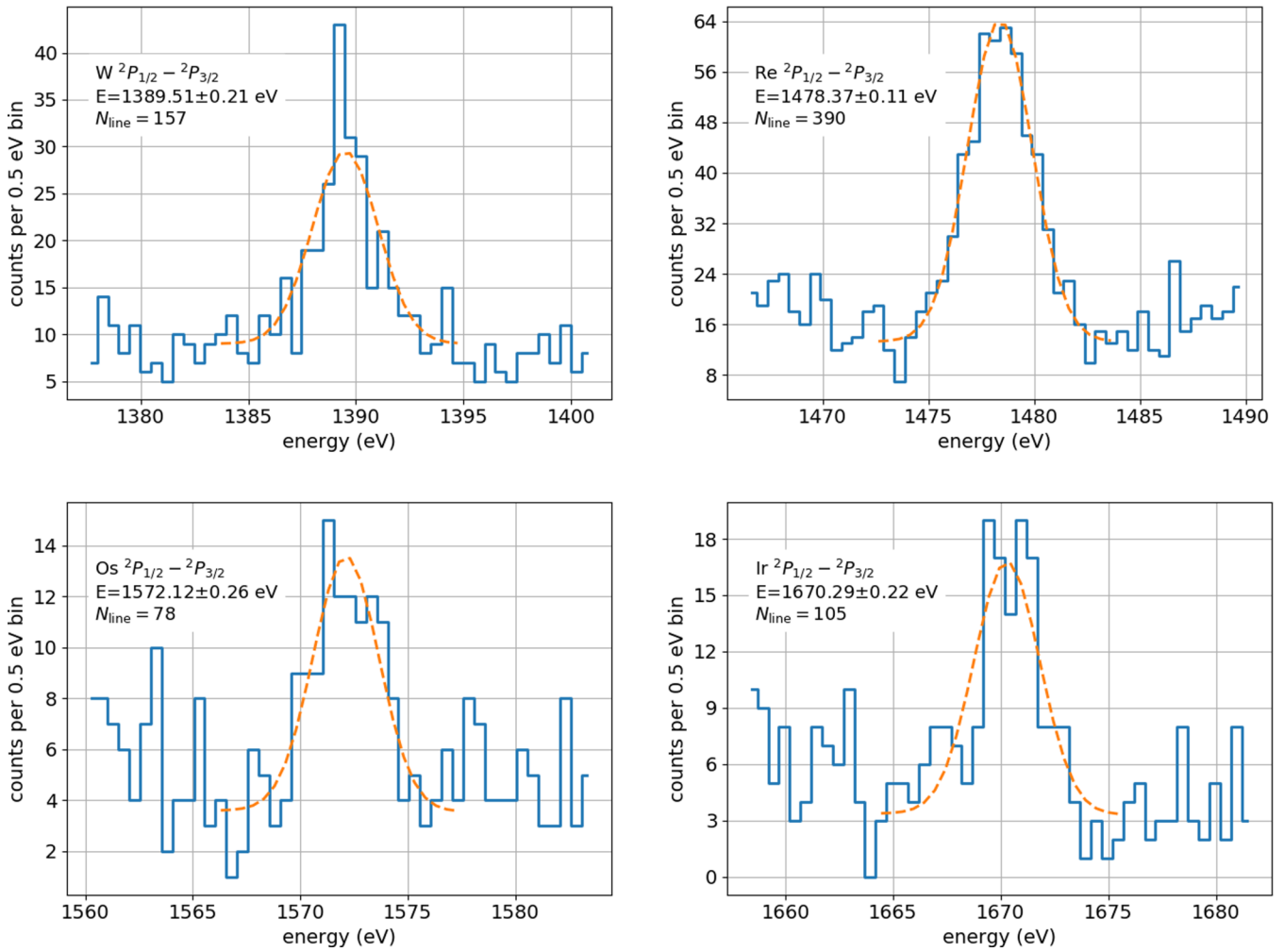

FIG. 3. X-ray spectra (blue) and fits (orange dashes) to Gaussian lineshapes with 3.6 eV FWHM resolution of the F-Like $^2P_{1/2}$-$^2P_{3/2}$ transition in Re, W, Ir, and Os as labeled on each subfigure. Data within 12 eV of the centroid is shown; the fit is done only with data within 6 eV of the centroid. The narrow fit range is chosen because the model of a flat background is more likely to be accurate over a narrow energy range. The Gaussian lineshape is dominated by the detector resolution; we predict a natural linewidth of 1.2×10^{-4} eV for Re, and similar values for the other nuclei. Text on each subfigure shows statistical uncertainty returned by the fitting routine, and the number of photons, N_{line}, in the line. The statistical uncertainty on the measurement centroid of a Gaussian distribution with N photons measured with standard deviation $\sigma \approx \text{FWHM}/2.355$ is $\sigma/\sqrt{N}$. For Re, with $N = 390$ photons, this uncertainty would be 0.08 eV; the uncertainty determined by the fit is slightly higher due to the finite background in the measurement.

For each pixel we create a *calibration curve* $E(c) = c/G(c)$, where E is the energy assigned to a photon that results in a corrected pulse height c, and G is the *gain*. A *calibration point*, a corresponding pair of corrected pulse height and energy, is determined by fitting a lineshape model to a histogram of corrected pulse heights. Here we use two such pairs, determined from the Al $K\alpha$ (1486 eV) line and the $2p$-$1s$ transition (1021 eV) in H-like Ne, and G is modeled as a linear function of c with the two free parameters determined by a fit to the calibration points. Al $K\alpha$ radiation was generated by x-ray illumination of the calibration target, while the Ne radiation was generated with the EBIT. The calibration spectra contain other well-known lines between the two calibration points from H-like and He-like Ne as well as the Mg $K\alpha$ line from the calibration target; we have used these additional lines to estimate the accuracy of this calibration approach in Appendix 2 and find it to be a small contribution to the total uncertainty. The Lorentzian widths, relative intensities, and peak energies of the $K\alpha_1$ and $K\alpha_2$ lines used to fit for the Al $K\alpha$ and Mg $K\alpha$ positions are from Ref. [19], and the lineshape used to fit for the position of the $2p$-$1s$ transition in H-like Ne is based on the energy levels in H-like Ne available from the NIST Atomic Spectra Database [17,20].

We determine the energy of the $^2P_{1/2}$-$^2P_{3/2}$ fine-structure transition in F-like Re, W, Os, and Ir by a fits to *co-added* histograms of x-ray energies, as shown in Fig. 3. Co-added histograms are generated by summing the histograms from the 126 pixels for which we measured an energy resolution of better than 4 eV at Al $K\alpha$. The transition was identified by looking for a spectral feature near the energy predicted by theory. When fitting, we fix the energy resolution to the value observed at nearby lines, and fix the background slope to zero. We take the uncertainty reported by the fitting routine to be the statistical uncertainty. The dominant source of systematic

TABLE II. The one-sigma contribution of the largest sources of systematic uncertainty in the Re, W, Os, and Ir spectra. All values have units of eV.

Source	Re	W	Os	Ir
Gain Drift	0.08	0.08	0.17	0.17
Calibration	0.04	0.04	0.04	0.04
Non-Gaussian response	0.01	0.03	0.12	0.02
Energy resolution	0.003	0.005	0.030	0.015

uncertainty in these measurements is from gain drift over time that remains even after analysis step (3) is performed. A detailed discussion of the systematic uncertainty is found in the Appendix, which includes a summary in Table II.

Os and Ir spectra

The Os and Ir data were taken two days later. On this day, we experienced power surges that caused us to re-initialize the NETS room temperature readout electronics multiple times. We later determined that this re-initialization was incomplete. The only negative effect of the incomplete re-initialization on the data was a reduction in count rate, because roughly half of the pixels in NETS failed to produce useful spectra. Due to the higher energy of the F-like $^2P_{1/2}$-$^2P_{3/2}$ fine-structure lines in Os and Ir, we changed the calibration target to primarily produce Al $K\alpha$ and Si $K\alpha$ (1740 eV) radiation, and we did not inject Ne into the EBIT. The steps used to produce spectra with the Os and Ir data analysis were identical to the Re analysis, except for the use of Al $K\alpha$ and Si $K\alpha$ for calibration, and the use of Si $K\alpha$ instead of Al $K\alpha$ for the correction steps. The Lorentzian widths, relative intensities, energies, and energy uncertainties of the Si $K\alpha_1$ and Si $K\alpha_2$ used for calibration fits are based on data from the laboratory notebook of Mooney provided by Szabo-Foster; the data were taken in 1990, the methods used to acquire the data were similar to those described in Ref. [19]. The Appendix contains additional details on the systematic uncertainty analysis, including how systematic uncertainties vary for each line.

III. DISCUSSION

The rigorous theoretical treatment of the QED radiative corrections in F-like ions has been recently presented in Ref. [6]. Here, we extend the computations to the ions measured in the present work that have not been evaluated in Ref. [6].

The theoretical calculations rely on an effective combination of two powerful methods, namely, the multiconfiguration Dirac-Fock (MCDF) method [21–23] and rigorous QED perturbation theory [24]. The MCDF method is based on the Dirac-Coulomb-Breit Hamiltonian given by (in units $e = \hbar = m_e = 1$)

$$\hat{H} = \sum_{i=1}^{N} [c\boldsymbol{\alpha}_i \cdot \boldsymbol{p}_i + (\beta_i - 1)c^2 - V_{\rm nuc}(r_i)] + \sum_{i<j}^{N} \left[\frac{1}{r_{ij}} - \frac{\boldsymbol{\alpha}_i \cdot \boldsymbol{\alpha}_j}{2r_{ij}} - \frac{(\boldsymbol{\alpha}_i \cdot \boldsymbol{r}_{ij})(\boldsymbol{\alpha}_j \cdot \boldsymbol{r}_{ij})}{2r_{ij}^2} \right]. \quad (1)$$

Here, i, j enumerate the electrons and N stands for the total number of electrons, $V_{\rm nuc}(r_i)$ is the potential of a two-parameter Fermi nuclear charge distribution, and $\boldsymbol{\alpha}$ and β are the Dirac matrices. The Dirac-Coulomb-Breit Hamiltonian allows us to evaluate atomic energies up to an order $(\alpha Z)^2$ (α is the fine-structure constant). The higher-order terms in (αZ), as well as the radiative corrections of an order α and higher, can be further accounted for within rigorous QED treatment (see, for example, Refs. [25–27]).

For the present work, we first make use of the recent MCDF results of Ref. [5]. These values have been evaluated with the GRASP2K package [23]. In addition to the Dirac-Hartree-Fock values, the calculation includes the correlation and frequency-independent Breit contributions. The method for accounting for these contributions is well understood and lies in the increase of the configuration space of many-electron wave functions. Here we note that the transition $^2P_{1/2}$-$^2P_{3/2}$ considered in the present work occurs within one configuration of a Layzer complex [28], which cancels to a large extent the correlations between the $^2P_{3/2}$ and $^2P_{1/2}$ states. This effect has been recently studied in Refs. [5,29]. Thus, the smallness of the correlation and an excellent agreement with the experiment found for light elements, where the higher-order and radiative corrections are negligible, allows one to conclude that the relative error in the transition energy due the correlation and frequency-independent Breit terms is on the order of 10^{-6} for Kr, W, Re, Os, Ir [5].

Continuing with the second method, the higher-order terms in (αZ) represent the corrections beyond the Dirac-Coulomb-Breit Hamiltonian [Eq. (1)]. These corrections originate from the full treatment of the photon propagator, i.e., the frequency dependence of the Breit operator, and from the processes of creation and annihilation of virtual electron-positron pairs. Both of these effects can be consistently taken into account only within the QED theory. Here, we add the frequency-dependent Breit term evaluated in Ref. [5]. This contribution was calculated within the single-configuration Dirac-Hartree-Fock approximation. This configuration is constructed from the spectroscopic orbitals, which provide physical energies. We estimate its uncertainty as well as higher-order corrections to be of an order $(\alpha Z)^3/Z^2$ multiplied by a factor of two. This estimation is based on a comparison of two-photon exchange diagrams evaluated within rigorous QED and Breit approximations for the similar case of the $^2P_{3/2}$-$^2P_{1/2}$ transition in B-like ions. This source of the uncertainty dominates the total theoretical error bars for W, Re, Os, and Ir ions. This uncertainty is not attributed to the QED contribution and, therefore, is not included in the uncertainty of the QED values of Ref. [6].

The calculations are performed within an extended Furry picture starting with the Kohn-Sham potential generated for the $^2P_{3/2}$ ground state. The one-loop self-energy and vacuum polarization together with the screened radiative corrections have been rigorously taken into account. The uncertainty of the higher-order screened diagrams is estimated to be $(\alpha/8\pi)(\alpha Z)^4/Z^2$ multiplied by a factor of five. This uncertainty dominates the total theoretical error bars for the Kr ion.

Figure 4 compares the QED corrections calculated with the presented theoretical method to the experimental values. The experimental QED correction is defined as the experimental

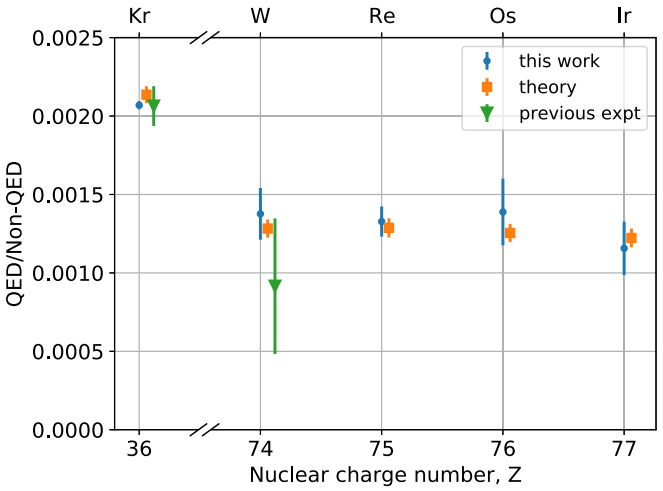

FIG. 4. Experimental QED correction as a fraction of the non-QED line energy compared with QED theory vs nuclear charge. Only elements studied in this work are shown, previous experiments are compiled in Ref. [6]. Points for the same nuclear charge are shifted horizontally for ease of comparison. Values and references to previous work are identical to Table I.

line energy less the non-QED theoretical value for the line energy. The largest difference found is 1.1σ in the case of Kr, where σ is the quadrature sum of the experimental statistical, experimental systematic, and theoretical uncertainty. All other differences are below 1σ.

It is valuable to have these measurements over narrow ranges in Z, such as our measurements of W, Re, Os, and Ir, because in some cases peculiar physical effects can cause strong dependence of atomic parameters on Z even over these narrow ranges. For example, it was recently predicted that the intensities of the electric-octupole $5s$-$5f$ transitions drop by about a factor of two between W and Ir due to cancellations in atomic matrix elements [30]. W was the only element measured between $Z = 40$ and $Z = 92$ among the previous experimental results reviewed in Ref. [6]. Here we improve on that measurement, and add three more measurements for similar Z. The excellent agreement between these measured and calculated transition energies provides strong validation of the theoretical methods used here.

IV. CONCLUSIONS

We have measured the $^2P_{3/2}$-$^2P_{1/2}$ transition energy in five F-like ions, three new (Re, Os, Ir), and two (Kr, W) with increased precision and accuracy. The relative uncertainty of these measurements ranged from 25 ppm for Kr to 210 ppm for Os. We also extended the rigorous QED treatment of this transition to the three new ions. We find excellent agreement between theory and experiment.

We use NETS, the microcalorimeter x-ray spectrometer, for high precision and accuracy line-energy measurement. We find NETS to be currently capable of ≈100 ppm uncertainty, with the dominate source of systematic uncertainty being gain drift over time. In the future we aim to reach 50 ppm or better through increasing collection time and reducing the effect of gain drift. We can better correct for the gain drift if we take calibration data simultaneously with science data. Further investigation into the drift mechanism may lead to modifications to decrease gain drift.

ACKNOWLEDGMENTS

Assistance provided by Csilla Szabo-Foster was greatly appreciated. This work was supported by the NIST Innovations in Measurement Science (IMS) Program and partially supported by the NIST Measurement Science and Engineering (MSE) Research Grant (No. 70NANB19H024) and the National Science Foundation (No. 1806494).

These data and the work were created by employees of the National Institute of Standards and Technology (NIST), an agency of the Federal Government. Pursuant to title 17 United States Code Section 105, works of NIST employees are not subject to copyright protection in the United States.

APPENDIX: Re ANALYSIS AND SYSTEMATICS

The NETS as it currently exists has multiple nonideal behaviors that lead to systematic uncertainties in line-position measurements. Other spectrometers that share a similar design with NETS exhibit similar nonidealities. Here we provide more detail on analysis steps, the underlying sources of systematics, and the steps we have taken to estimate the magnitude of these uncertainties in the analysis of the Re line position. In each section we identify how the determination of systematics for other lines differs from the Re line.

1. Gain drift over time

In NETS the ratio of pulse-height to energy at a particular x-ray photon energy is referred to as the *gain*. The gain drifts by roughly one part in 10^4 per hour. The reasons for this gain drift are not fully understood, although a significant portion is attributed to the cryogenic design in which the temperature of the nominally 1 K temperature stage changes by nearly a factor of two during a measurement [8]. As described in the text, we attempt to remove this drift by a combination of measuring calibration lines frequently, and assuming a smooth variation in pulse height as function of time. One source of systematic uncertainty, which we refer to as *gain drift*, is any gain variation left uncorrected by this process. We estimate the contribution of gain drift to the systematic uncertainty by looking for variation in the position of multiple calibration lines after our attempts to remove the drift. Figure 5 (top) shows the *energy inaccuracy* of the Al $K\alpha$ line vs time throughout the Re and W measurements. Energy inaccuracy is defined as the difference between the line position determined from a fit to a NETS spectrum and the literature line position. We believe the gain is a slowly varying function of time, possibly influenced by external disturbances to the NETS cryostat. Therefore, we expect that the gain variation would be poorly modeled by a Gaussian distribution. We attempt to compensate by estimating the gain drift uncertainty with a method more sensitive to outliers than a standard deviation calculation. We estimate the gain drift contribution to the systematic uncertainty as half of the peak-to-peak variation seen in Fig. 5 (top). The gain drift uncertainty was determined

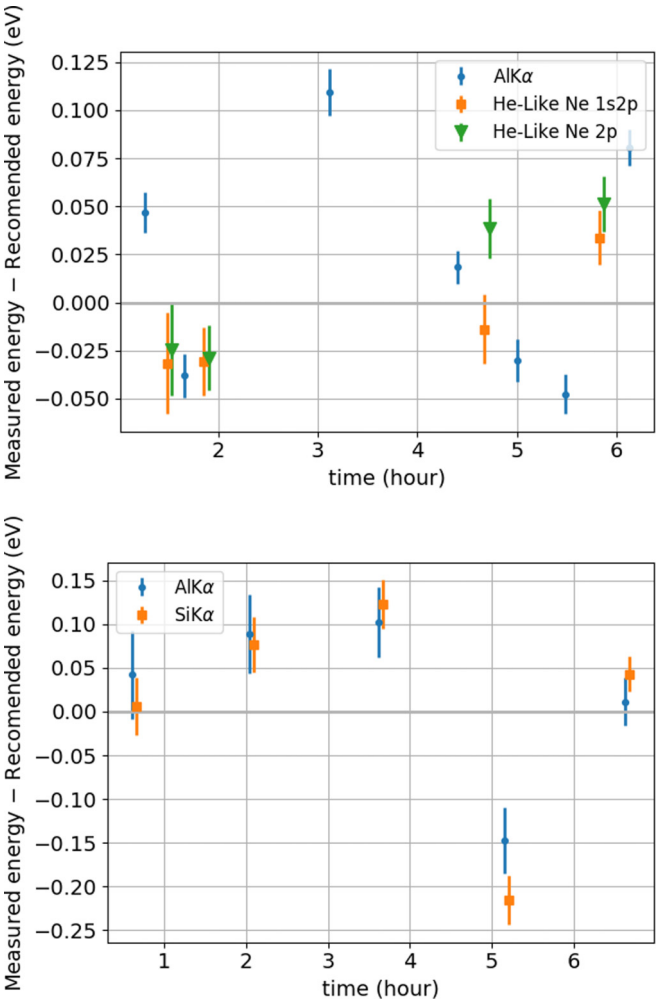

FIG. 5. NETS energy inaccuracy vs time the for calibration data acquired on the same day and used for the (top) Re and W measurements and (bottom) for the Ir and Os measurements. Each point for the Al and Si $K\alpha$ lines represents one time the calibration source was run for approximately 15 minutes, and each point for the He-like lines represents one time that Ne was injected into the EBIT. For each day we estimate the one-sigma systematic uncertainty associated with uncorrected gain drift as half of the peak-to-peak energy inaccuracy.

in a similar fashion for the Ir and Os data by using the data shown in Fig. 5 (bottom).

2. Calibration

The calibration curve of a TES is a nonlinear function of pulse height. So far, the highest-accuracy energy measurements with TES spectrometers [31,32] have used empirical calibration, as used in this work, rather than one at least partially derived from the device physics. The accuracy of the empirical calibration curve is poorer when calibration points are spaced further in energy. Here we estimate the accuracy of the empirical calibration used for the Re and W analysis by using well-known lines in our spectra that were not used to generate the calibration curve. The energy inaccuracy measured at each line is shown in Fig. 6. A weighted

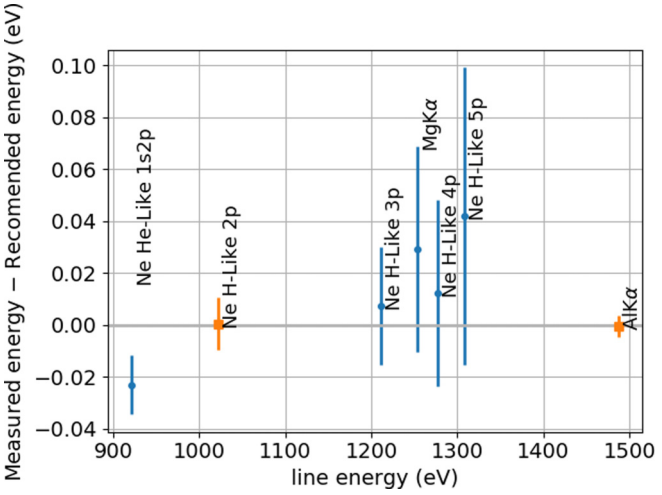

FIG. 6. NETS energy inaccuracy vs line energy for the well-known lines present calibration spectra used for the W and Re data. Lines used for calibration are orange squares. The errors bars show only the fit uncertainty. We expect the calibration to be most accurate between the two calibration points, and we find that all line inaccuracies between the calibration points are consistent with zero.

average of the energy inaccuracy of the four lines between the calibration points is 0.02 ± 0.02 eV. At the one-sigma level, the calibration bias is bounded by the range 0.0 to 0.04 eV. Because this range is small compared with other sources of uncertainty, we approximate it as a symmetric uncertainty with value 0.04 eV. We cannot repeat this analysis for Os and Ir due to the lack of well-known lines between the calibration points used in that analysis. The energies of interest are quite similar, so we use the same uncertainty in both cases.

The accuracy of the empirical calibration curve can also be limited by uncertainty on the calibration points. The published uncertainties are 0.010 eV for Al $K\alpha$ [19] and 0.019 eV for Si $K\alpha$ lines. The uncertainty of the Si $K\alpha$ line is taken from the same private communication previously described. The uncertainty on the energy position of the H-like Ne $2p$ lineshape is ≈0.003 eV. These values are comparable to or smaller the value from the empirical test, so we use the value from the empirical test unmodified.

The NETS data show better than 50 ppm calibration accuracy with a two-point calibration over a 50% energy bandwidth. The success of the two-point calibration is likely due to the large ratio, ≈7, of saturation energy to the energies of interest. Previous x-ray TES work with comparable accuracy has required four or more points for calibration, when the same ratio was ≈2 [31,32].

H-like Ne 2p lineshape

The H-like Ne $2p$ lineshape we measure contains unresolved substructure due to the finite resolution of NETS. The effective uncertainty of the energy position of the lineshape is determined by considering uncertainties on the energies and relative intensities of the constituent lines. Due to the relatively low nuclear charge and simple atomic structure of H-like Ne, the energy levels are calculated to the 10^{-5} eV level from QED theory [20]. We measure a combination of

radiation from the relaxation of the $2p_{1/2}$ and $2p_{3/2}$ levels which are about 0.45 eV apart, and the relaxation rate should be independent of angular momentum. For the EBIT conditions, the main population mechanism for both levels is the direct excitation from the ground state, which leads to an expected population ratio of 1 : 2. Simulation of the EBIT conditions we used yield a ratio of 1 : 1.99. The $2s_{1/2}$ level is at a similar energy, but we do not expect it to contribute because the primary radiative decay channel is about six orders of magnitude weaker than for the $2p$ states. Therefore we model the lineshape with two Lorentzians corresponding to the $^2P_{1/2}$ and $^2P_{3/2}$ levels, with an intensity ratio of 1 : 2, and estimate that the energy uncertainty is ≈0.003 eV.

3. Energy-resolution uncertainty

The number of photons observed in the F-like $^2P_{1/2}$-$^2P_{3/2}$ line is low enough that allowing the detector energy resolution to be a free parameter was deemed unwise. We do not know the exact energy resolution at this line, but we do have measurements at many nearby lines. We found values of energy resolution varying from 3.5 to 3.7 eV over the many well-known lines we were able to fit. We fit the F-like $^2P_{1/2}$-$^2P_{3/2}$ line positions with a fixed value of 3.6 eV and reported the resulting values in this work. We repeated the fits with an energy resolution of 3.8 eV and took the difference between these two fits as an estimate of the energy resolution contribution to the systematic uncertainty. We found values ranging from 0.003 eV for Re to 0.030 eV for Os.

4. Non-Gaussian detector response

The pixels in the NETS have a slightly non-Gaussian detector response. Recent work on this topic found a low-energy tail due to electron escape in the same pixels used in the NETS spectrometer. This low-energy tail accounts for at most 4% of the counts in a given line [8,33]. All of the fits reported outside of this section use a purely Gaussian response function. We do not have tail parameter measurements at the energies of interest. We repeated the entire analysis procedure with plausible tail parameters ($f_{\text{tail}} = 0.024$, $l_{\text{tail}} = 8$ eV) based on Ref. [33] and found that the F-like $^2P_{1/2}$-$^2P_{3/2}$ line shifts of 0.03 eV for W, 0.01 eV for Re, 0.12 for Os, and 0.02 eV for Ir. We believe the value for Os is larger both because it has the fewest observed photons, and there appear to be some other lines ≈10 eV below the line of interest. We use these shifts as values for the systematic uncertainty associated with the detector response function.

[1] J. D. Gillaspy, Highly charged ions, J. Phys. B: At., Mol. Opt. Phys. **34**, R93 (2001).

[2] J. D. Gillaspy, D. Osin, Yu. Ralchenko, J. Reader, and S. A. Blundell, Transition energies of the D lines in Na-like ions, Phys. Rev. A **87**, 062503 (2013).

[3] J. Sapirstein and K. T. Cheng, *s*-matrix calculations of energy levels of the lithium isoelectronic sequence, Phys. Rev. A **83**, 012504 (2011).

[4] P. Indelicato, QED tests with highly charged ions, J. Phys. B: At., Mol. Opt. Phys. **52**, 232001 (2019).

[5] M. C. Li, R. Si, T. Brage, R. Hutton, and Y. M. Zou, Proposal of highly accurate tests of breit and QED effects in the ground state $2p^5$ of the F-like isoelectronic sequence, Phys. Rev. A **98**, 020502(R) (2018).

[6] A. V. Volotka, M. Bilal, R. Beerwerth, X. Ma, T. Stöhlker, and S. Fritzsche, QED radiative corrections to the $^2P_{1/2}$-$^2P_{3/2}$ fine structure in fluorinelike ions, Phys. Rev. A **100**, 010502(R) (2019).

[7] V. M. Shabaev, I. I. Tupitsyn, M. Y. Kaygorodov, Y. S. Kozhedub, A. V. Malyshev, and D. V. Mironova, QED corrections to the $^2P_{1/2}$ - $^2P_{3/2}$ fine structure in fluorinelike ions: Model Lamb shift operator approach, Phys. Rev. A **101**, 052502 (2020).

[8] P. Szypryt, G. C. O'Neil, E. Takacs, J. N. Tan, S. W. Buechele, A. S. Naing, D. A. Bennett, W. B. Doriese, M. Durkin, J. W. Fowler, J. D. Gard, G. C. Hilton, K. M. Morgan, C. D. Reintsema, D. R. Schmidt, D. S. Swetz, J. N. Ullom, and Y. Ralchenko, A transition-edge sensor-based x-ray spectrometer for the study of highly charged ions at the National Institute of Standards and Technology electron beam ion trap, Rev. Sci. Instrum. **90**, 123107 (2019).

[9] J. Clementson, P. Beiersdorfer, G. V. Brown, M. F. Gu, H. Lundberg, Y. Podpaly, and E. Träbert, Tungsten spectroscopy at the Livermore electron beam ion trap facility, Can. J. Phys. **89**, 571 (2011).

[10] B. Denne, E. Hinnov, J. Ramette, and B. Saoutic, Spectrum lines of Kr XXVIII–Kr XXXIV observed in the JET tokamak, Phys. Rev. A **40**, 1488 (1989).

[11] J. D. Gillaspy, Y. Aglitskiy, E. Bell, C. M. Brown, C. Chantler, R. D. Deslattes, U. Feldman, L. Hudson, J. M. Laming, E. S. Meyer, C. A. Morgan, J. R. Roberts, F. G. Serpa, J. Sugar, and E. Takacs, First results from the EBIT at NIST, Phys. Scr. **1997**, 99 (1997).

[12] M. A. Levine, R. E. Marrs, J. R. Henderson, D. A. Knapp, and M. B. Schneider, The electron beam ion trap: A new instrument for atomic physics measurements, Phys. Scr. **1988**, 157 (1988).

[13] B. Blagojević, E.-O. Le Bigot, K. Fahy, A. Aguilar, K. Makonyi, E. Takács, J. N. Tan, J. M. Pomeroy, J. H. Burnett, J. D. Gillaspy, and J. R. Roberts, A high efficiency ultrahigh vacuum compatible flat field spectrometer for extreme ultraviolet wavelengths, Rev. Sci. Instrum. **76**, 083102 (2005).

[14] R. Silwal, E. Takacs, J. M. Dreiling, J. D. Gillaspy, and Yu. Ralchenko, Identification and plasma diagnostics study of extreme ultraviolet transitions in highly charged yttrium, Atoms **5**, 30 (2017).

[15] R. Silwal, A. Lapierre, J. D. Gillaspy, J. M. Dreiling, S. A. Blundell, Dipti, A. Borovik, G. Gwinner, A. C. C. Villari, Y. Ralchenko, and E. Takacs, Measuring the difference in nuclear charge radius of Xe isotopes by EUV spectroscopy of highly charged Na-like ions, Phys. Rev. A **98**, 052502 (2018).

[16] G. E. Holland, C. N. Boyer, J. F. Seely, J. N. Tan, J. M. Pomeroy, and J. D. Gillaspy, Low jitter metal vapor vacuum arc ion source for electron beam ion trap injections, Rev. Sci. Instrum. **76**, 073304 (2005).

[17] A. Kramida, Yu. Ralchenko, J. Reader, and NIST ASD Team, NIST Atomic Spectra Database (ver. 5.7.1) [Online]. Available:

https://physics.nist.gov/asd [2020, July 27]. National Institute of Standards and Technology, Gaithersburg, MD (2019).

[18] J. W. Fowler, B. K. Alpert, W. B. Doriese, Y. I. Joe, G. C. O'Neil, J. N. Ullom, and D. S. Swetz, The practice of pulse processing, J. Low Temp. Phys. **184**, 374 (2016).

[19] J. Schweppe, R. D. Deslattes, T. Mooney, and C. J. Powell, Accurate measurement of Mg and Al $K\alpha_{1,2}$ x-ray energy profiles, J. Electron Spectrosc. Relat. Phenom. **67**, 463 (1994).

[20] G. W. Erickson, Energy levels of one-electron atoms, J. Phys. Chem. Ref. Data **6**, 831 (1977).

[21] J. P. Desclaux, A multiconfiguration relativistic Dirac-Fock program, Comput. Phys. Commun. **9**, 31 (1975).

[22] F. A. Parpia, C. F. Fischer, and I. P. Grant, GRASP92: A package for large-scale relativistic atomic structure calculations, Comput. Phys. Commun. **175**, 745 (2006).

[23] P. Jönsson, G. Gaigalas, J. Bieroń, C. F. Fischer, and I. P. Grant, New version: GRASP2k relativistic atomic structure package, Comput. Phys. Commun. **184**, 2197 (2013).

[24] V. M. Shabaev, Two-time Green's function method in quantum electrodynamics of high-Z few-electron atoms, Phys. Rep. **356**, 119 (2002).

[25] A. N. Artemyev, V. M. Shabaev, I. I. Tupitsyn, G. Plunien, and V. A. Yerokhin, QED Calculation of the $2P_{3/2}$-$2P_{1/2}$ Transition Energy in Boronlike Argon, Phys. Rev. Lett. **98**, 173004 (2007).

[26] Y. S. Kozhedub, A. V. Volotka, A. N. Artemyev, D. A. Glazov, G. Plunien, V. M. Shabaev, I. I. Tupitsyn, and T. Stöhlker, Relativistic recoil, electron-correlation, and QED effects on the $2p_j$-$2s$ transition energies in Li-like ions, Phys. Rev. A **81**, 042513 (2010).

[27] A. V. Malyshev, A. V. Volotka, D. A. Glazov, I. I. Tupitsyn, V. M. Shabaev, and G. Plunien, QED calculation of the ground-state energy of berylliumlike ions, Phys. Rev. A **90**, 062517 (2014).

[28] D. Layzer, On a screening theory of atomic spectra, Ann. Phys. (NY) **8**, 271 (1959).

[29] R. Si, X. L. Guo, T. Brage, C. Y. Chen, R. Hutton, and C. F. Fischer, Breit and QED effects on the $3d^{92}D_{3/2}\rightarrow{}^2D_{5/2}$ transition energy in Co-like ions, Phys. Rev. A **98**, 012504 (2018).

[30] H. A. Sakaue, D. Kato, I. Murakami, H. Ohashi, and N. Nakamura, Observation of electric octupole emission lines strongly enhanced by the anomalous behavior of a cascading contribution, Phys. Rev. A **100**, 052515 (2019).

[31] J. W. Fowler, B. K. Alpert, D. A. Bennett, W. B. Doriese, J. D. Gard, G. C. Hilton, L. T. Hudson, Y.-I. Joe, K. M. Morgan, G. C. O'Neil, C. D. Reintsema, D. R. Schmidt, D. S. Swetz, C. I. Szabó, and J. N. Ullom, A reassessment of absolute energies of the x-ray L lines of lanthanide metals, Metrologia **54**, 494 (2017).

[32] H. Tatsuno, W. B. Doriese, D. A. Bennett, C. Curceanu, J. W. Fowler, J. Gard, F. P. Gustafsson, T. Hashimoto, R. S. Hayano, J. P. Hays-Wehle, G. C. Hilton, M. Iliescu, S. Ishimoto, K. Itahashi, M. Iwasaki, K. Kuwabara, Y. Ma, J. Marton, H. Noda, G. C. O'Neil *et al.*, Absolute energy calibration of x-ray TESs with 0.04 eV uncertainty at 6.4 keV in a hadron-beam environment, J. Low Temp. Phys. **184**, 930 (2016).

[33] G. C. O'Neil, P. Szypryt, E. Takacs, J. N. Tan, S. W. Buechele, A. S. Naing, Y. I. Joe, D. Swetz, D. R. Schmidt, W. B. Doriese, J. D. Gard, C. D. Reintsema, J. N. Ullom, J. S. Villarrubia, and Yu. Ralchenko, On low-energy tail distortions in the detector response function of x-ray microcalorimeter spectrometers, J. Low Temp. Phys. **199**, 1046 (2019).